Structure of MsbA from *E. coli*: A Homolog of the Multidrug Resistance ATP Binding Cassette (ABC) Transporters

Geoffrey Chang* and Christopher B. Roth

Multidrug resistance (MDR) is a serious medical problem and presents a major challenge to the treatment of disease and the development of novel therapeutics. ABC transporters that are associated with multidrug resistance (MDR-ABC transporters) translocate hydrophobic drugs and lipids from the inner to the outer leaflet of the cell membrane. To better elucidate the structural basis for the "flip-flop" mechanism of substrate movement across the lipid bilayer, we have determined the structure of the lipid flippase MsbA from *Escherichia coli* by x-ray crystallography to a resolution of 4.5 angstroms. MsbA is organized as a homodimer with each subunit containing six transmembrane α-helices and a nucleotide-binding domain. The asymmetric distribution of charged residues lining a central chamber suggests a general mechanism for the translocation of substrate by MsbA and other MDR-ABC transporters. The structure of MsbA can serve as a model for the MDR-ABC transporters that confer multidrug resistance to cancer cells and infectious microorganisms.

The increasing incidence of multidrug resistance is a significant health problem that has profoundly impacted the treatment of infectious diseases and cancer. The World Health Organization has recently reported that multidrug-resistant bacteria can account for up to 60% of all hospital-acquired infections globally (*1*). Multidrug resistance in the treatment of cancer is responsible for tens of thousands of deaths per year. Multidrug resistance can be conferred by a number of transporters that pump drugs out of cells. Certain multidrug resistance transporters such as the human P-glycoprotein, MDR1, can transport a diverse class of amphipathic drug molecules (*2*). There is evidence that some of these drug transporters may act as phospholipid flippases and it has been proposed that multidrug transporters may function as drug flippases, translocating drugs from the inner to the outer leaflet of the lipid bilayer. In an effort to understand the structural basis of multidrug resistance, we have determined the crystal structure of the multidrug resistance transporter homolog, MsbA, from *Escherichia coli* (Eco-msbA). The msbA gene product belongs to a superfamily of transporters that contain an adenosine triphosphate (ATP) binding cassette (ABC), which is also called a nucleotide-binding domain (NBD) (*3, 4*). ABC transporters translocate a wide variety of substrates, including amino acids, peptides, ions, sugars, toxins, lipids, and drugs and are implicated in a number of serious human diseases, including cystic fibrosis and several disorders of the immune system (*5–7*).

MsbA is a member of the MDR-ABC transporter group by sequence homology and is more closely related to the mammalian P-glycoproteins than any other bacterial ABC transporter (*8, 9*). Although LmrA from *Lactococcus lactis* is functionally more similar to the P-glycoproteins, MsbA is even more conserved by sequence homology (*10, 11*). MDR-ABC transporters have been proposed to act as "hydrophobic vacuum cleaners" because of their ability to remove lipids and drugs from the inner membrane leaflet (*12*). MsbA transports lipid A, a major component of the bacterial outer cell membrane, and is the only bacterial ABC transporter that is essential for cell viability (*13*). Loss of MsbA from the cell membrane or a mutation that disrupts transport results in a lethal accumulation of lipid A in the cytoplasmic leaflet (*14, 15*). Several bacterial homologs of msbA that include the flippase ValA from *Francisella novicida* and LmrA, have been reported in over 30 divergent prokaryotic species (*16*).

The overall organization of MsbA is consistent with most bacterial MDR-ABC transporters and its amino acid sequence is remarkably similar to several mammalian P-glycoproteins involved in multidrug resistance. All known ABC transporters are composed of four modules, including two membrane spanning regions and two NBDs. Unlike the mammalian P-glycoproteins, which have these components fused into a single polypeptide, the msbA gene encodes a half transporter that contains a single membrane spanning region fused with a NBD. MsbA is assembled as a homodimer with a total molecular mass of 129.2 kD. Hydropathy analysis indicates six membrane spanning regions with the NBD located on the cytoplasmic side of the cell membrane (*17*). The primary role of the transmembrane domain is to recognize and transport substrates across the lipid bilayer. The ABC, which is the hallmark of the MDR-ABC transporter family and is located in the NBD, couples the energy of ATP hydrolysis to substrate translocation. Although the NBD structures of the histidine transporter (HisP), the maltose transporter (MalK), the DNA repair enzyme (Rad50), and the branched-chain amino acid transporter from *Methanococcus jannaschii* (MJ1267) have been determined, the structural basis for substrate translocation through the cell membrane is not clear (*18–21*).

The structure of MsbA establishes the general architecture of the MDR-ABC transporter family, and facilitates our understanding of the fundamental flipping mechanism that moves hydrophobic substrates from the inner to the outer membrane leaflet. The protein sequence of Eco-msbA is 36 and 32% identical to the NH_2-terminal and COOH-terminal halves of human MDR1, respectively (Fig. 1) (*22*). Human MDR3, which is a phosphatidylcholine flippase and is 73% identical in protein sequence to human MDR1, is 31% identical in protein sequence to Eco-msbA (*23*). The similarity in protein sequence and function between MsbA and human MDR1/MDR3 suggests a common evolutionary origin and, therefore, they may have common mechanisms by which they catalyze the flipping of substrates. The crystal structure of Eco-msbA determined to 4.5 Å in resolution provides a framework for deciphering P-glycoproteins and suggests a general mechanism for the transport of substrate across the lipid bilayer.

Structure determination. Membrane protein x-ray crystallography of transporters and ion channels presents new challenges owing to the disorder caused by detergent and the inherent movement of transmembrane α-helices. We have, therefore, adopted a strategy of rapidly exploring crystallization space by cloning, overexpressing, and purifying more than 20 full-length bacterial transporters and their homologs derived from several MDR-ABC transporter families and 12 bacterial species (*24*). Our expectation was that one or more of these natural variants would be more optimal for protein expression, purification, and crystal formation. Each full-length MDR-ABC transporter was cloned and recombinantly expressed in a BL21 strain of *E. coli* (*25*). Although func-

Department of Molecular Biology, MB-9, The Scripps Research Institute, La Jolla, CA 92037, USA.

*To whom correspondence should be addressed. E-mail: gchang@scripps.edu

tional activity of the purified material was not assayed, the integrity of each transporter dimer was confirmed by gel filtration. After screening and refining approximately 96,000 crystallization conditions for several MDR-ABC transporters and their homologs using ~20 detergents, we obtained more than 35 distinct membrane protein crystal forms. The MsbA MDR-ABC transporter from *E. coli* yielded crystals of good diffraction quality that were used for x-ray structure determination.

Eco-msbA crystallized in space group P1 (a = 107.8 Å, b = 126.1 Å, c = 206.6 Å, α = 83.5°, β = 76.3°, γ = 84.1°) using dodecyl-α-D-maltoside (α-DDM) (Table 1) (*26*). The native crystals diffracted to a resolution of ~6.2 Å using synchotron radiation but data was fairly anisotropic. In an effort to strengthen protein lattice contacts and decrease the disorder within these crystals, we applied a crystal refinement strategy that included the screening of an extensive matrix of detergents, detergent concentrations, salts, temperatures, organics, additives, deuterium oxide, and heavy metals. One compound, $OsCl_3$, significantly improved the diffraction quality to a limiting resolution of 4.5 Å. This compound was later found to bind at crystal lattice contacts between NBDs of

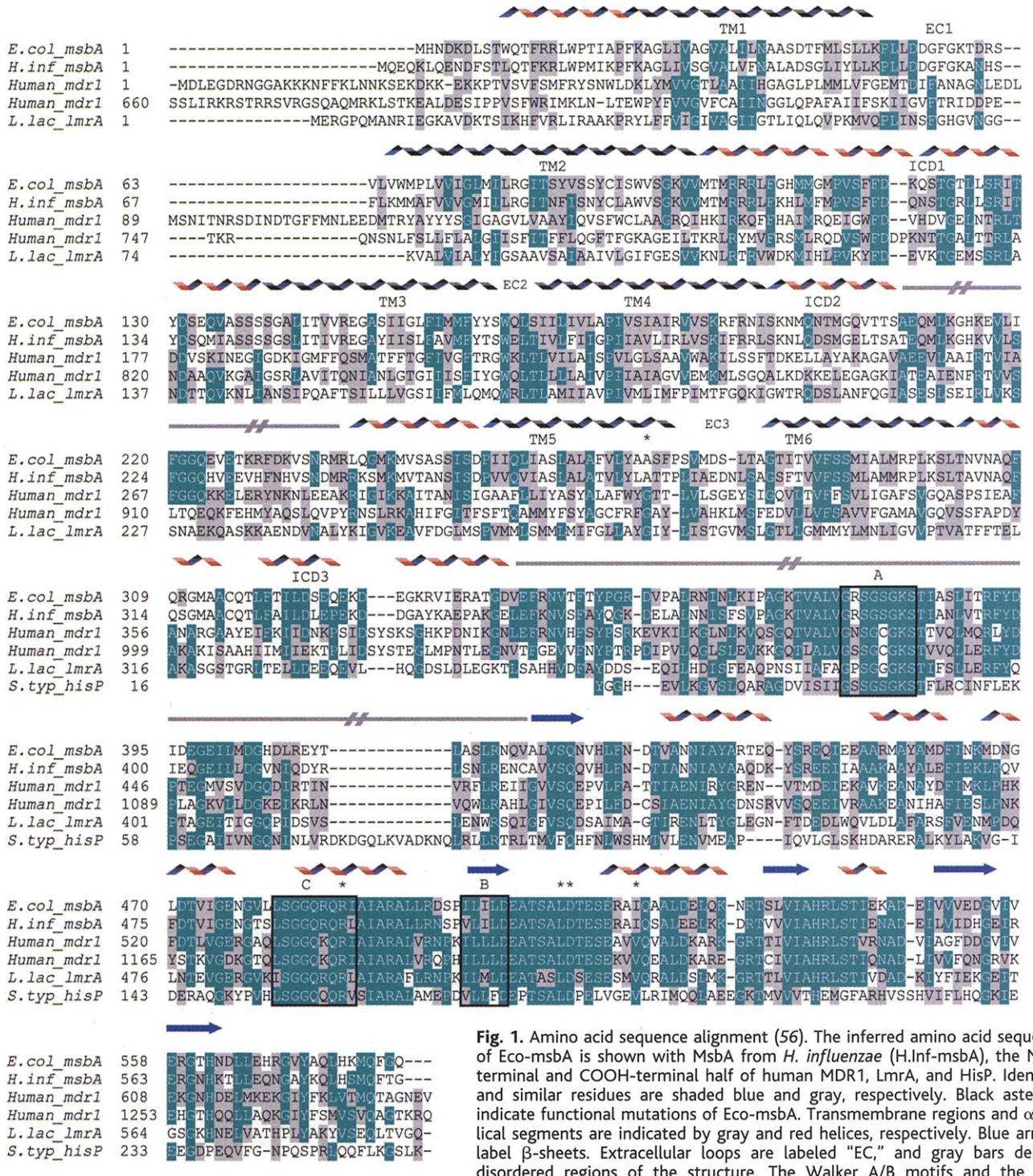

Fig. 1. Amino acid sequence alignment (*56*). The inferred amino acid sequence of Eco-msbA is shown with MsbA from *H. influenzae* (H.Inf-msbA), the NH_2-terminal and COOH-terminal half of human MDR1, LmrA, and HisP. Identical and similar residues are shaded blue and gray, respectively. Black asterisks indicate functional mutations of Eco-msbA. Transmembrane regions and α-helical segments are indicated by gray and red helices, respectively. Blue arrows label β-sheets. Extracellular loops are labeled "EC," and gray bars denote disordered regions of the structure. The Walker A/B motifs and the ABC signature motif regions are boxed and labeled by A, B, and C, respectively. Alignment was done with the program ClustalW (*50*).

one transporter pair (Fig. 2). In view of the improved diffraction quality, data collected from this soaked crystal was used as the "native" data set for x-ray structure determination. Protein phases were determined by the method of single isomorphous replacement and single anomalous scattering (SIR/SAS) using two evenly split fragments from a single crystal and also by phase combination with a two-wavelength multiple anomalous dispersion (MAD) using the computer package PHASES (*27, 28*). Iterative eightfold noncrystallographic symmetry averaging, solvent flattening/flipping, phase extension, and amplitude sharpening using in-house programs yielded electron density maps of excellent quality for tracing a polypeptide chain (Fig. 3) (*29*). A chemical model was built using the program CHAIN (*30*), and the protein sequence registration was established by the presence of electron density for bulky aromatic groups in the transmembrane helices (Fig. 3C). Regions of the HisP model were useful as a guide for building the NBD.

The structure refinement of Eco-msbA was complicated by a rapid decrease in the intensity of the diffraction pattern as a function of resolution, corresponding to an overall temperature factor of ~150 Å^2. Similar temperature factors were reported for the K^+ ion channel from *Streptomyces lividans* (KcsA) (*31*) as well as for the mechanosensitive ion channel from *Mycobacterium tuberculosis* (Tb-mscL) (*32*). The experimentally phased electron density maps, however, appeared to be of much higher quality than one would expect for this temperature factor (*33*). This suggested that there were predominant orientations for the transporters in the crystal that were likely stabilized by heavy-atom binding with additional orientations that introduced a degree of positional disorder. As a consequence, whereas the diffraction pattern remained relatively strong at lower resolution, the scattering contributions from this ensemble of transporters and associated detergent interfered at higher resolution, resulting in a rapid decrease in diffraction intensities to a higher angle of diffraction resolution. Standard crystallographic refinement protocols are generally inadequate for modeling this type of positional disorder and, as a result, we were unable to refine a single model of Eco-msbA to values of R and R_{free} below ~38 and ~45%, respectively. In an effort to better simulate the data, 16 copies of the asymmetric unit (eight molecules per asymmetric unit) were simultaneously refined against the $OsCl_3$ data (Set 2) with very strict eightfold noncrystallographic harmonic constraints (2000 kcal/mol) between the monomers using the program XPLOR (*34–38*). After

Table 1. Data collection and crystallographic analysis. Diffraction data used in the structural analysis were collected from single crystals at beamlines 11-1 (λ = 0.98 Å) and 9-2 for the multiwavelength experiments at the Stanford Synchotron Radiation Laboratory (SSRL). Additional data sets were collected at beamline 5.0.2 at the Advanced Light Source (ALS) and on laboratory x-ray sources (MAR300/MAR345). Crystals were translated periodically during the data collection to adjust for the rapid decay due to radiation damage. All data sets were collected at −165°C and processed using the programs HKL2000 (HKL Research) and MOSFLM/SCALA (*49*). The concentration of PEG 300 was gradually increased to 29% by vapor diffusion for optimal cryo-protection for flash-cooling in liquid nitrogen or propane. The concentration of α-DDM and $OsCl_3$ was critical for maintaining the integrity and diffraction quality of the crystals.

Parameter	Native	$OsCl_3$ crystal 1 (λ=0.980 Å)	$OsCl_3$ crystal 1 (λ=1.139 Å)	$OsCl_3$ crystal 1 (λ=1.140 Å)	$OsCl_3$ crystal 2 (λ=0.980 Å)
		Diffraction data			
Bragg spacing limits (Å)	80-6.2	80-5.75	80-5.4	80-6.2	80-4.5
Total observations	197,870	150,453	192,102	185,241	384,156
Unique observations	25,367	29,009	30,157	26,145	69,609
R_{sym} (%)	4.7%	4.1%	6.7%	6.2%	4.6%
Completeness	90%	99%	96%	98%	90%

Generation of experimental electron density	
Phasing power ($OsCl_3$)	2.4
Density correlation coefficient between pairs of monomers in asymmetric unit	36% lowest 64% highest
Overall figure of merit	0.7

Refinement statistics		*Model geometry*	
Single model		Bond length deviation	0.009 Å
R factor (80.0–4.5 Å)	38%	Bond angle deviation	1.8°
R_{free} (80.0–4.5 Å)	45%		
Sixteen models			
R factor (80.0–4.5 Å)	27%		
R_{free} (80.0–4.5 Å)	38%		
Overall B factor of the model	90 Å^2		

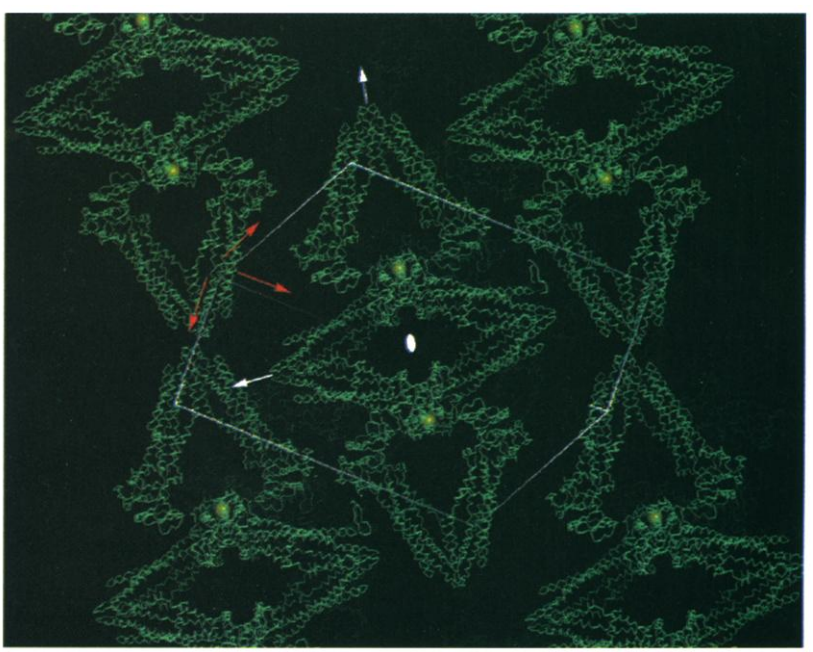

Fig. 2. Crystal packing diagram of Eco-msbA transporters (chain trace in green). This orientation shows the pseudo-222 noncrystallographic symmetry. White arrows indicate the direction of the pseudo twofold operators relating monomers within a MsbA transporter. The space group is P1 and the unit cell is superimposed onto the crystal lattice. Yellow spheres indicate $OsCl_3$ bound at contacts between two Eco-msbA transporters, which improved diffraction. The image was generated with the program INSIGHTII (MSI, San Diego, California).

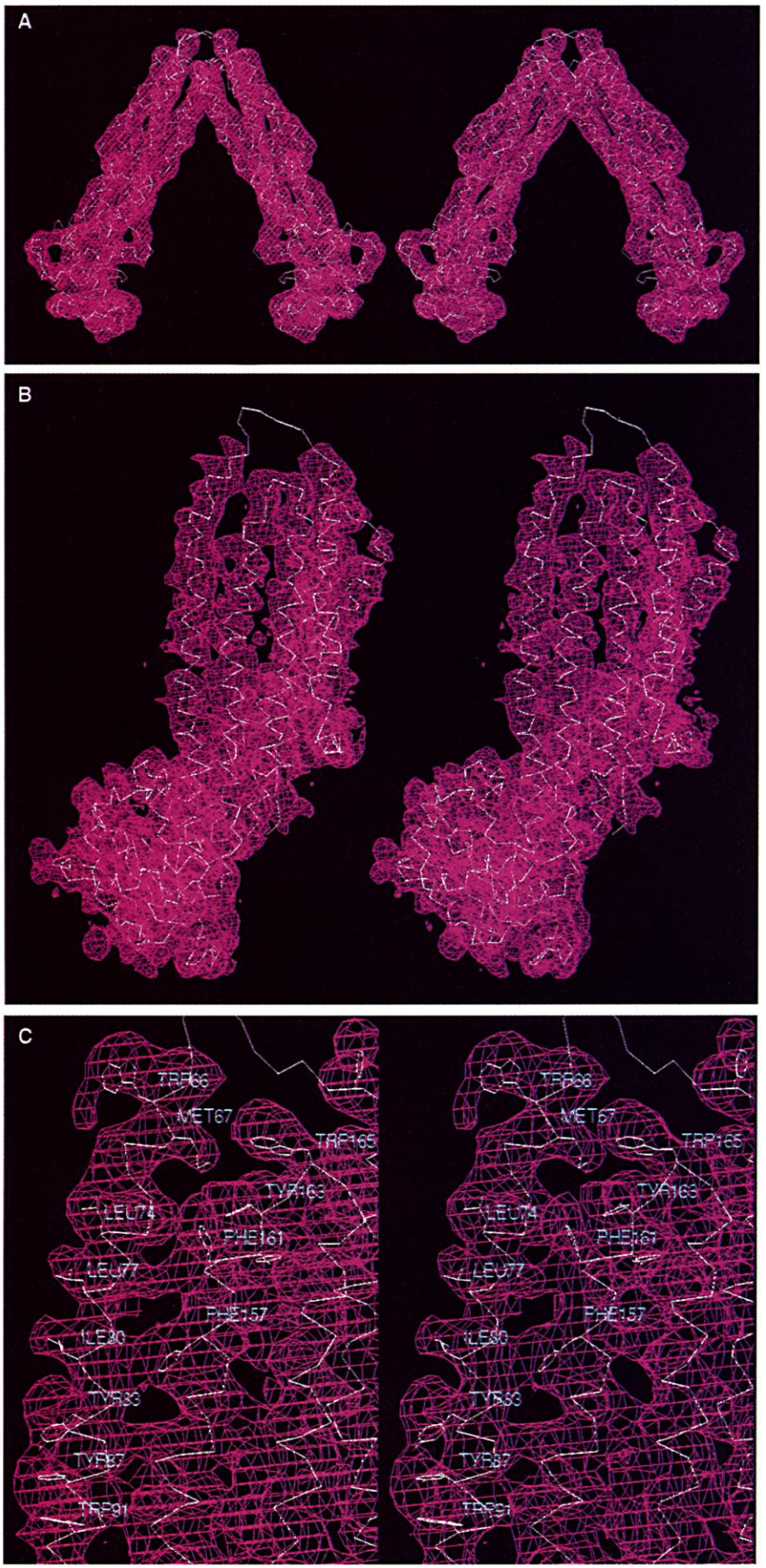

molecular dynamics refinement, an ensemble of very similar models (average root mean square deviation of C_a atoms among models of <1.4 Å) was achieved with a crystallographic R value of 27% and an R_{free} of 38%. Residue positions in helical regions were well defined in these models, whereas the loop regions were less ordered. An averaged model with good stereochemistry was computed and used for structural analysis.

Structural organization of Eco-MsbA. The crystal structure of Eco-msbA transporter is consistent with the molecule being a homodimer and each subunit is composed of two domains (Fig. 4). We have identified a third domain bridging the transmembrane and nucleotide-binding domains. Eco-msbA is approximately 120 Å in length, with the transmembrane domain, including the membrane spanning region, accounting for ~52 Å. All the transmembrane α-helices are tilted between 30° and 40° from the normal of the membrane, forming a cone shaped structure with two substantial openings on either side facing the lipid bilayer. These openings are ~25 Å wide in the longest dimension and lead into a large cone-shaped chamber in the interior of the molecule's transmembrane domain. The outer membrane leaflet half of the transmembrane domain forms the intermolecular contacts holding the two monomers of the transporter together. The dimer interface, which is mostly contributed by the transmembrane helices, buries approximately 850 Å^2 of solvent accessible surface area. The base of the chamber facing the cytoplasm is ~45 Å in the widest dimension and the volume of the chamber can easily accommodate a lipid A molecule. The resolved regions of the NBDs share no intermolecular contact and are separated by ~50 Å in the closest dimension.

Transmembrane domain structure. Eco-msbA begins with the NH_2-terminus on the cytoplasmic side as a helix (residues 10 to 21) that is parallel with the lipid bilayer (Fig. 4). Residues Trp^{10}, Phe^{13}, and Trp^{17} would intercalate the inner leaflet side of the cell membrane. The polypeptide chain continues into the first transmembrane helix (TM1, residues 22 to 52) and

Fig. 3. Stereoviews of Eco-msbA experimental electron density at 4.5 Å resolution. The C_α polypeptide trace is superimposed on the electron density and calculated at 1.5 σ. View looking (**A**) into and (**B**) perpendicular to the chamber opening. (B) Shows sharpened electron density of the transmembrane domain, intracellular domain, and the NBD. (**C**) Shows a close up of sharpened electron density containing modeled bulky side chains revealing α-helical structural features and registration of the polypeptide backbone. The densities were rendered with the program CHAIN.

leads into the first extracellular loop (EC1, residues 53 to 64), which crosses over to the far side of the transporter. The electron densities for residues 58 to 63 of EC1 are diffuse. The second transmembrane helix (TM2, residues 65 to 96) forms part of the opening of the flippase chamber and appears mobile when comparing TM2 α-helices from other copies of Eco-msbA in the unit cell. The third and fourth transmembrane helices (TM3, residues 140 to 164, and TM4, residues 168 to 192, respectively) are connected by a very short extracellular loop (EC2, residues 165 to 167), which has polar character. Strong electron density is present for several bulky residues, which include Phe^{161}, Tyr^{162}, and Tyr^{163} in TM3 and Trp^{165} in EC2 (Fig. 3C). The fifth transmembrane helix (TM5, residues 253 to 272) begins with a kink caused by Pro^{253} and forms half of the opening facing the bilayer. TM5 is connected to the sixth transmembrane helix (TM6, residues 281 to 301) by an extracellular loop (EC3, residues 273 to 280). Although the absolute orientation of Eco-msbA in the membrane is not known, the putative third extracellular loop (EC3) in human MDR1 aligns by sequence homology to Eco-msbA EC3 and has been shown to be located on the cell surface by in vivo topology studies using the antibody UIC2 (*39*). TM2 and TM5 from opposing monomers within the dimer form the major dimerization contact and are well positioned to serve as a hinge, allowing the transporter to undergo significant structural rearrangements.

NBD structure. The NBD (colored cyan in Fig. 4) is the most conserved feature of the MDR-ABC transporter family and contains the Walker A/B motif along with the ABC signature motif. In the absence of ATP or nucleotide analog in this structure, residues 341 to 418, which includes the Walker A motif, are disordered in our electron density maps. The crystal packing, however, suggests sufficient vol-

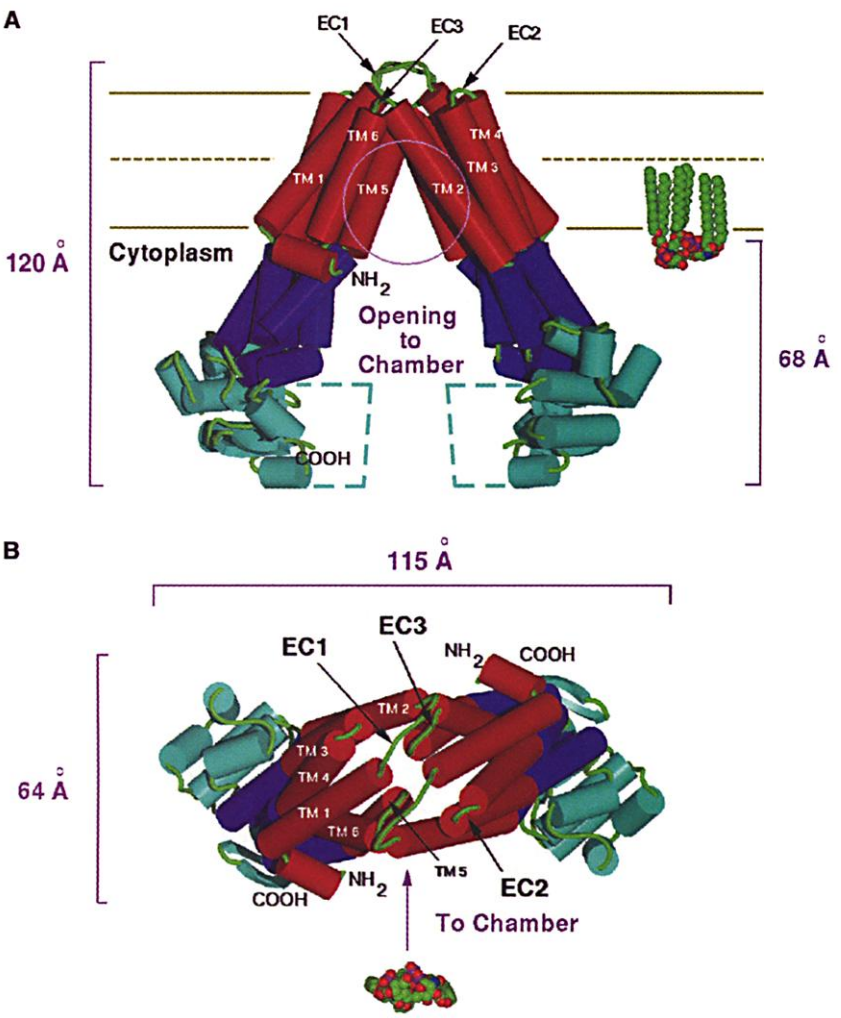

Fig. 4. Structure of Eco-msbA. (**A**) View of dimer looking into the chamber opening. The transmembrane domain, NBD, and intracellular domain are colored red, cyan, and dark blue, respectively. Transmembrane α-helices are marked and the connecting loops are shown in green. A model of lipid A (not in the crystal structure) is shown to the right, embedded in the lower bilayer leaflet. Solid and dotted green lines represent the boundaries of the membrane bilayer leaflets. Dotted cyan lines indicate the approximate location of the disordered region in the NBD. (**B**) View of Eco-msbA from extracellular side, perpendicular to the membrane with model of lipid A. Transporter dimensions are labeled and images were rendered using BOBSCRIPT and RASTER 3D (*51–53*).

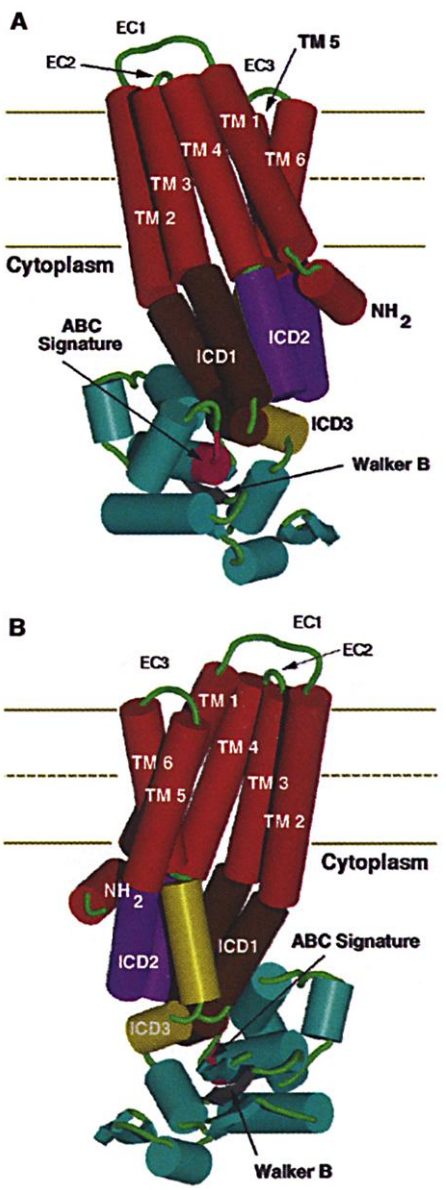

Fig. 5. View of Eco-msbA looking (**A**) from the lipid bilayer at the external (embedded) surface of the chamber opening and (**B**) looking at the interior of the chamber. The transmembrane domain is colored red and the transmembrane α-helices are marked. The NBD is colored cyan, with the Walker B motif and ABC signature motif highlighted in gray and pink. ICD1, ICD2, and ICD3 are colored brown, violet, and yellow for clarity. The estimated cell membrane (~35 Å) and the boundary between the bilayer leaflets are illustrated as solid and dotted yellow lines. Figure was rendered using BOBSCRIPT and RASTER 3D (*51–53*).

ume to accommodate the mass of the Walker A region. The remaining portion of the NBD is well resolved in our structure and includes an α-helix (residues 331 to 340) and residues 418 to 564, which contains the ABC signature motif (colored pink in Fig. 5) and the Walker B region (colored gray in Fig. 5). The NBD of Eco-msbA has significant similarity in sequence and structure to the corresponding regions found in HisP with an rms deviation of ~1.5 Å (C_α) for residues 445 to 528. NBD residues that are in direct contact with the intracellular domain (residues 420 to 448, 500 to 508, and 531 to 556) are among some of the most highly conserved regions among all members of the MDR-ABC transporter family. The COOH-terminus end of Eco-msbA (residues 565 to 582) is not resolved.

Intracellular domain (ICD) structure. A distinctive feature of the MDR-ABC transporter family is two extensive intracellular regions called ICD1 (residues 97 to 139) and ICD2 (residues 193 to 252). We have identified a third intracellular subdomain that connects TM6 with the NBD that we label ICD3 (residues 302 to 327). We collectively designate the region located between the transmembrane domain and the NBD as the intracellular domain (colored dark blue in Fig. 4). Most of the residues that correspond to structural elements in ICD1 that are in contact with either the transmembrane domain or the NBD are highly conserved throughout the MDR-ABC transporter family. ICD1 (colored brown in Fig. 5), which is sandwiched between ICD2 (colored violet in Fig. 5) and the NBD, is composed of three α-helices connected by short loops to form a "U"-like structure. The second α-helix of ICD1 (residues 111 to 121) is highly conserved and is nestled against residues 420 to 430 of the NBD. The well-ordered portions of ICD2 in our electron density maps are mostly α-helical (residues 193 to 207 and 237 to 252). The electron densities for residues 208 to 236, however, are diffuse within the crystal. ICD3 links TM6 and the NBD and forms two α-helices connected by short loops (colored yellow in Fig. 5B). The α-helix just preceding the NBD domain (residues 318 to 327) is conserved among MDR-ABC transporters and is in direct contact with both ICD1 and ICD2.

Chamber structure. The chamber is a symmetric structure that is formed from two Eco-msbA transmembrane domains and extends along the pseudo twofold axis perpendicular to the cell membrane (Fig. 6A). The chamber has an opening (~25 Å) on either side facing the bilayer providing free access of substrate from the cytoplasmic leaflet of the lipid bilayer while excluding molecules from the outer leaflet. The openings to the chamber are defined by intermolecular interactions between TM2 of one monomer and TM5 of another (Fig. 4A). Residues 268 to 273 of TM2 lining the opening of the chamber are partially shielded from the bilayer by TM5. The residues lining the chamber are contributed by all 12 transmembrane α-helices and could be highly solvated. The inner membrane leaflet side of the chamber contains a cluster of positively-charged residues (Arg^{148}, Arg^{183}, Lys^{187}, Arg^{190}, Lys^{194}, and Arg^{296}) (Fig. 6B), which contrasts with the significantly less charged and more hydrophobic environment within the outer membrane leaflet side.

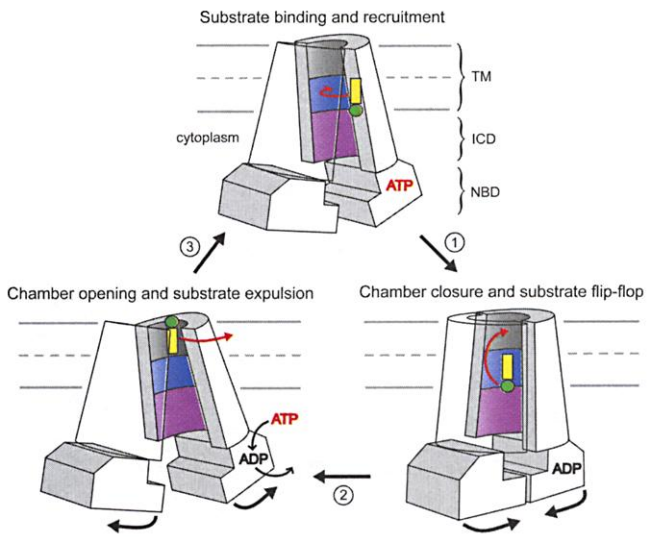

Fig. 7. Potential model for lipid A transport by Eco-msbA. Stages 1 to 3 begin at top and proceeds clockwise. See text for details. (1) Lipid A binding, triggering of ATP hydrolysis, and recruitment of substrate to chamber. (2) Closure of the chamber and translocation of lipid A. Interaction between the two NBDs is possible. (3) Opening of the chamber, movement of TM2/TM5, release of lipid A to the outer bilayer leaflet, and nucleotide exchange. A small yellow rectangle and a green circle denote the hydrophobic tails and sugar head groups of lipid A, respectively. The transmembrane domain (TM), intracellular domain (ICD), and nucleotide-binding domain (NBD) are labeled. The cell membrane is represented as a set of two horizontal lines separated by a dash to indicate the separation of bilayer leaflets. Blue regions indicate positive charge lining the chamber, and purple regions represent the intracellular domain. The gray region on the outer membrane side of the chamber is hydrophobic. Red and black arrows show the movement of substrate and the structural changes of MsbA, respectively.

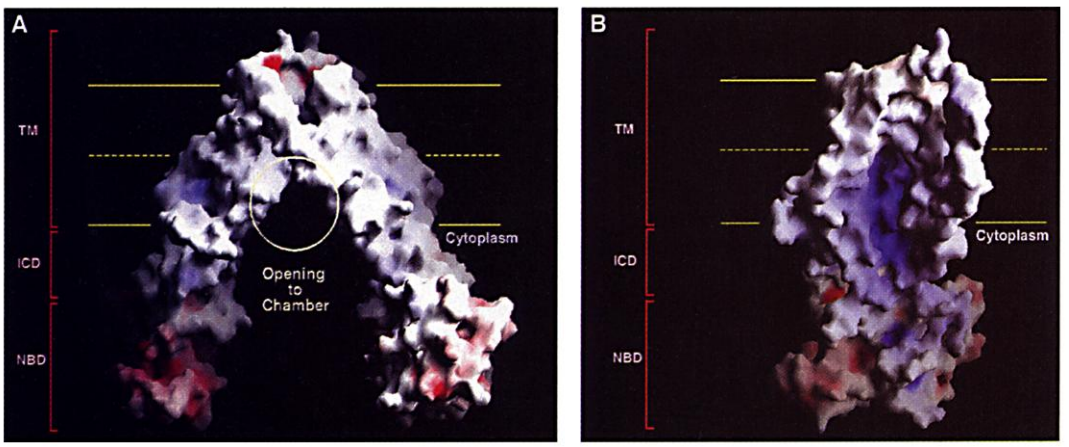

Fig. 6. Molecular surface rendering of Eco-msbA with electrostatic potentials. This figure was generated with the program GRASP (*54*), assuming an ionic strength of 100 mM NaCl and dielectric constant of 2 and 80 for protein and solvent, respectively. The surface potential varies continuously from blue (positive) to red (negative). The cell membrane, which is ~35 Å wide, is represented with yellow lines. The transmembrane domain (TMD), intracellular domain (ICD), and NBD are indicated. (**A**) Side view of dimer looking into the chamber. The opening of the chamber spans the lower bilayer leaflet. (**B**) View of Eco-msbA monomer looking at the inner surface of the chamber. The surface potential within the lower half of the chamber is highly positive due to a clustering of lysine and arginine residues.

Possible flipping mechanism. The structure of MsbA suggests a general mechanism for hydrophobic substrate translocation by members of the MDR-ABC transporter group (Fig. 7). Studies of P-glycoprotein function indicate that residues lining the proposed chamber opening (TM2, TM5, and TM6) play an important role in substrate recognition (*40*). There is significant evidence indicating a cooperative interaction between the two opposing NBDs (*41*). The extensive contact of the intracellular domain (colored purple in Fig. 7) with both the transmembrane domain and the NBD allow it to function as a conduit coupling the triggering of ATP hydrolysis by the NBD to tertiary arrangements of the transmembrane α-helices. Upon binding of a lipid A molecule, conformational changes relayed from the transmembrane domain to the intracellular domain initiate nucleotide hydrolysis by the NBD (step 1 in Fig. 7). Movement of TM2, TM5, TM6, and the two nucleotide-binding domains serves to recruit the substrate and close the chamber (step 2 in Fig. 7). Hydrolysis of ATP by the NBD may result in a conformational shift that promotes the interaction of the adjacent NBDs. The cluster of charges lining the chamber on the inner membrane leaflet side creates an energetically unfavorable microenvironment for a hydrophobic substrate. The asymmetric charge distribution in the interior of the chamber is consistent with the vectored transport of substrate from the inner to the outer membrane leaflet. Faced with both the charge and the highly polar contribution of potentially bound solvent, the lipid A molecule "flips" into an energetically more favorable position within the outer membrane leaflet side of the chamber (colored gray in Fig. 7) where it can form hydrophobic interactions. The substrate is now properly orientated to enter the outer bilayer leaflet. The flipping of substrate signals the chamber to undergo structural rearrangements that include the separation of the NBDs and repositioning of TM2 and TM5, enabling the expulsion of the substrate to the outer membrane leaflet (step 3 in Fig. 7). Alternatively, it has been proposed that some drug transporters can extrude their substrates directly into the extracellular medium from the inner leaflet of the bilayer (*42*). Substrate release signals the NBD to exchange ATP for ADP, resetting the system. This entropically driven "flip-flop" mechanism could account for the unusually broad range of hydrophobic drugs and lipids transported by members of the MDR-ABC transporter family. Several other variations of this mechanism are plausible and will be refined using biochemical and structural information derived from additional MsbA studies.

Although we believe that MsbA may not be able to serve as a close structural representative of the ABC transporters that translocate hydrophilic substrates, there is significant evidence that suggests that human MDR1 and other MDR-ABC transporters share transport mechanisms and structural components similar to Eco-msbA (*43*). First and foremost, human MDR1, mouse MDR3, and LmrA are lipid flippases like Eco-msbA and transport short-chain lipids (*44*), phosphatidylcholine (*45*), and phophatidylethanolamine (PE) (*46*), respectively. Secondly, the size and shape of the chamber of Eco-msbA could accommodate and transport a wide variety of amphipathic molecules, which explains why human MDR1 and mouse MDR3 can extrude an unusually broad range of substrates. Finally, the transport kinetics of P-glycoproteins reconstituted in lipid vesicles deviate significantly from those made for "pore-like" transport systems (*47, 48*). The explanation is now apparent. The crystal structure reveals that Eco-msbA is not a pore through the cell membrane but is a molecular machine scanning the lower bilayer leaflet for substrates, accepting them laterally, and flipping them to the outer membrane leaflet. The x-ray structure of Eco-msbA provides a foundation for understanding the bioenergetics of lipid/drug "flip-flop" for the entire MDR-ABC transporter family. The structure can also help elucidate the mechanism underlying the multidrug resistance phenotype, which could have a profound impact on the development of novel therapeutics used to treat cancer and infectious disease.

References and Notes

1. "Drug Resistance Threatens to Reverse Medical Progress," WHO Press Release 41 (World Health Organization, Geneva, Switzerland, 2000).
2. C. Chen *et al.*, *Cell* **47**, 3 (1986).
3. B. Sarkadi, E. M. Price, R. C. Boucher, U. A. Germann, G. A. Scarborough, *J. Biol. Chem.* **267**, 7 (1992).
4. S. V. Ambudkar *et al.*, *Proc. Natl. Acad. Sci. U.S.A.* **89**, 18 (1992).
5. I. B. Holland, M. A. Blight, *J. Mol. Biol.* **293**, 2 (1999).
6. C. M. Fuller, D. J. Benos, *Am. J. Physiol.* **263** (no. 2, part 1), C267 (1992).
7. J. Trowsdale *et al.*, *Nature* **348**, 6303 (1990).
8. K. Tomii, M. Kanehisa, *Genome Res.* **8**, 1048 (1998).
9. A. L. Hughes, *Mol. Biol. Evol.* **11**, 6 (1994).
10. H. W. van Veen *et al.*, *Nature* **391**, 6664 (1998).
11. For the purpose of this work, which focuses on using MsbA as a structural model, we use sequence homology as a basis for grouping MsbA with the MDR-ABC transporters. By sequence identity calculated with the program BLAST, MsbA is 32% and LmrA is 30% identical to the NH_2-terminal half of human MDR1.
12. Y. Raviv, H. Pollard, E. P. Bruggermann, I. Pastan, M. M. Gottesman, *J. Biol. Chem.* **265**, 7 (1990).
13. M. Karow, C. Georgopoulos, *Mol. Microbiol.* **7**, 1 (1993).
14. Z. Zhou, K. A. White, A. Polissi, C. Georgopoulos, C. R. Raetz, *J. Biol. Chem.* **273**, 20 (1998).
15. W. T. Doerrler, M. C. Reedy, C. R. Raetz, *J. Biol. Chem.* **276**, 15 (2001).
16. M. K. McDonald, S. C. Cowley, F. E. Nano, *J. Bacteriol.* **179**, 24 (1997).
17. B. Rost, P. Fariselli, R. Casadio, *Protein Sci.* **5**, 8 (1996).
18. L. W. Hung *et al.*, *Nature* **396**, 6712 (1998).
19. J. Diez *et al.*, *J. Mol. Biol.* **305**, 4 (2001).
20. K. P. Hopfner *et al.*, *Cell* **101**, 7 (2000).
21. N. Karpowich *et al.*, *Structure* **9**, 7 (2001).
22. S. F. Altschul, W. Gish, W. Miller, E. W. Myers, D. J. Lipman, *J. Mol. Biol.* **215**, 3 (1990).
23. J. J. Smit *et al.*, *Cell* **75**, 3 (1993).
24. The nucleotide sequence of *E. coli* msbA used for cloning was obtained from the published genomic sequence of *E. coli* K-12, locus AE000193.1:9950..11698 as defined by the NCBI Entrez database. The predicted translation of Eco-msbA produces a 582–amino acid polypeptide with a molecular weight of 64,461 and was confirmed to within 0.07% by mass spectrometry. MsbA homologs and other putative MDR-ABC transporters were identified using a BLAST search of the NCBI microbial genomes database, using the amino acid sequence of msbA predicted from the *E. coli* gene. Clones were isolated by polymerase chain reaction from purified genomic DNA of several bacterial species including *E. coli*, *Bacillus subtilis*, *Vibrio cholerae*, *Actinobacillus actinomycetemcomitans*, *Haemophilus influenzae*, *Helicobacter pylori*, *Klebsiella pneumoniae*, *Streptococcus pneumoniae*, *Pseudomonas aeruginosa*, *Enterococcus faecalis*, *Pasteurella multocida*, *Salmonella typhimurium*, *S. paratyphi*, and *Chlorobium tepidum*.
25. MsbA homologs were cloned into the pET19b expression vector (Novagen, Madison, WI), which contains a 23-residue fusion leader containing an NH_2-terminal deca-histidine tag. Clones were expressed in *E. coli* BL21(DE3) (Novagen, Madison, WI) in a 50-liter batch fermentor at 37°C using 2 mM IPTG (Anatrace, Maumie, OH) as an inducer. Eco-msbA protein was extracted from ~1 kg of *E. coli* by agitation in the presence of 1% dodecyl-α-D-maltoside (α-DDM). Extracted MsbA was purified in the presence of 20 mM Tris-HCl (pH 7.5), 20 mM NaCl, and 0.05% α-DDM using nickel-chelate and ion-exchange chromatography. Purified Eco-msbA was assayed for purity by Coomassie blue staining and mass spectrometry, and then concentrated to 10 to 15 mg/ml protein with a final detergent concentration of 0.05% α-DDM.
26. Crystallization trials were performed using a multivariate crystallization matrix of temperatures, detergents, precipitants, salts, and additives. The best Eco-msbA crystals were obtained using the sitting drop method at 5°C, by combining protein with precipitant at a ratio of 1 to 3:1. The precipitant solution consisted of 20 mM tris-HCl (pH 7.5), 100 to 200 mM citrate (pH 4.8 to 5.4), 15 to 20% PEG 300, 80 to 120 mM Li_2SO_4, and 0.05% α-DDM. Crystals appeared within 3 weeks and continued to grow for 2 months to a full size of (0.4 mm by 0.8 mm by 0.3 mm). To verify identity, crystals were washed and dissolved, and NH_2-terminal amino acid sequence was determined to five residues. Mass spectrometry analysis confirmed the predicted molecular weight.
27. W. Furey, S. Swaminathan, *Methods Enzymol.* **277**, 590 (1997).
28. Initial electron density maps clearly revealed that the asymmetric unit contained four complete Eco-msbA transporters (eight monomers) in a pseudo-222 arrangement consistent with the operators in the self-rotation function and corresponding to a solvent/detergent content of ~75%. Electron density correlations on experimentally derived maps indicated that there were some differences between the transporters that did and did not bind osmium heavy atoms. Transporters that did not bind $OsCl_3$ did not adhere to a perfect twofold relating monomers within a dimer. These differences were accommodated in the averaging masks and density modifications.
29. The package PHASES was used for all phase calculations with multiple isomorphous and all anomalous scattering data. The isomorphous and anomalous difference Pattersons yielded strong peaks (>21 σ) for the $OsCl_3$ sites. The correct hand of the structure was established by observing the hand of the α-helices in the sharpened 4.5 Å electron density map and also confirmed when

docking a fragment of the hisP to the NBD density. The initial experimentally phased electron density map revealed eight monomers of Eco-msbA with real-space correlation coefficient ranging from 36 to 64% between monomers. Eightfold noncrystallographic symmetry averaging, solvent flattening/flipping, phase extension, and amplitude sharpening were accomplished using locally written software (G. Chang, unpublished data) and yielded electron density maps that were of excellent quality for model building. The final inversion R value of 38% reflects the relatively large solvent content, the intensity distribution of the data, the disorder due to the missing regions of the molecule, and the presence of detergent in the crystal.

30. J. S. Sacks, *J. Mol. Graphics* **6**, 224 (1988).
31. D. A. Doyle *et al.*, *Science* **280**, 69 (1998).
32. G. Chang, R. H. Spencer, A. T. Lee, M. T. Barclay, D. C. Rees, *Science* **282**, 5397 (1998).
33. Numerous rounds of vector refinement were performed using the program XPLOR to best fit the model into the sharpened electron density. Using this preliminary model, anisotropic correction to the diffraction was applied using XPLOR. Wilson plots indicated a sharp drop of the mean diffraction intensities as a function of resolution with an overall B factor for the data ~150 Å^2.
34. M. Pellegrini, N. Gronbech-Jensen, J. A. Kelly, G. M. Pfluegl, T. O. Yeates, *Proteins* **29**, 426 (1997).
35. P. Gros, W. F. van Gunsteren, W. G. J. Hol, *Science* **235**, 458 (1987).
36. J. Kuriyan *et al.*, *Proteins* **10**, 340 (1991).
37. A. T. Brünger, J. Kuriyan, M. Karplus, *Science* **235**, 458 (1987).
38. Multicopy refinements were done using 5, 8, 10, or 16 copies of the asymmetric unit. These multicopy refinements yielded similar crystallographic R factors (27%), R_{free} values (38%), and averaged model structures. The significant drop in the R_{free} value during the multicopy refinements and the similarity of the independently averaged model structures suggested a proper fit of the data. The choice of using 16 copies of the asymmetric unit provided an opportunity to more finely observe their spatial distribution. Helical regions were more similar while loop regions were generally more disordered. B factors for all atoms were fixed at 90 Å^2 during the multicopy refinement. An image of superimposed models (C_α traces) generated from the multicopy refinement can be found on *Science* Online (www.sciencemag.org/cgi/content/full/293/5536/1793/DC1).
39. Y. Zhou, M. M. Gottesman, I. Pastan, *Arch. Biochem. Biophys.* **367**, 1 (1999).
40. S. V. Ambudkar *et al.*, *Annu. Rev. Pharmacol. Toxicol.* **39**, 361 (1999).
41. A. Senior, S. Bhagat, *Biochemistry* **37**, 3 (1998).
42. H. Bolhuis *et al.*, *EMBO J.* **15**, 4239 (1996).
43. C. F. Higgins, M. M.Gottesman, *Trends Biosci.* **17**, 1 (1992).
44. A. van Helvoort *et al.*, *Cell* **87**, 3 (1996).
45. A. J. Smith *et al.*, *FEBS Lett.* **354**, 3 (1994).
46. A. Margolles, M. Putman, H. W. van Veen, W. K. Konings, *Biochemistry* **38**, 49 (1999).
47. M. Horio, M. M.Gottesman, I. Pastan, *Proc. Natl. Acad. Sci. U.S.A.* **85**, 10 (1988).
48. D. F. Cano-Gauci, F. S. Seibert, A. R. Safa, J. R. Riordan, *Biochem. Biophys. Res. Commun.* **209**, 2 (1995).
49. S. Bailey, CCP4 Project, *Acta Crystallogr. D* **50**, 760 (1994).
50. J. D. Thompson, D. G. Higgins, T. J. Gibson, *Nucleic Acids Res.* **22**, 22 (1994).
51. R. M. Esnouf, *J. Mol. Graphics* **15**, 132 (1997).
52. P. J. Kraulis, *J. Appl. Crystallogr.* **24**, 946 (1991).
53. E. A. Merritt, D. J. Bacon, *Methods Enzymol.* **277**, 505 (1997).
54. B. Honig, A. Nicholls, *Science* **268**, 1144 (1995).
55. We thank M. Elsliger for computer support in the multicopy refinement and X. Dai for assisting in the processing of the diffraction data. We thank H. Banie, C. McCarthy, and M. Hornsby for technical assistance. We also thank the staff at the Stanford Synchrotron Radiation Laboratory (SSRL), the Advanced Light Source (ALS), the Cornell High Energy Synchrotron Source (CHESS), and the Advanced Photon Source (APS) for their help in the data collection and screening of a couple thousand MDR-ABC transporter crystals. We thank I. Wilson, J. Johnson, R. Milligan, W. Balch, P. Wright, and C. Higgins for thoughtful discussions. We thank P. Wright, J. Kelly, and R. Lerner for supporting membrane protein x-ray crystallography at The Scripps Research Institute (TSRI). This project was supported by start-up lab funds from TSRI, the NIH (GM61905-01), and the Presidential Early Career Award for Scientists and Engineers (PECASE). Coordinates have been deposited with Protein Data Bank (accession code 1JSQ).
56. Single-letter abbreviations for the amino acid residues are as follows: A, Ala; C, Cys; D, Asp; E, Glu; F, Phe; G, Gly; H, His; I, Ile; K, Lys; L, Leu; M, Met; N, Asn; P, Pro; Q, Gln; R, Arg; S, Ser; T, Thr; V, Val; W, Trp; and Y, Tyr.

6 July 2001; accepted 6 August 2001

REPORTS

Hydrogen 21-Centimeter Emission from a Galaxy at Cosmological Distance

M. A. Zwaan,[1]* P. G. van Dokkum,[2] M. A. W. Verheijen[3,4]

We have detected the neutral atomic hydrogen (HI) emission line at a cosmologically significant distance [redshift (z) = 0.18] in the rich galaxy cluster Abell 2218 with the Westerbork Synthesis Radio Telescope. The HI emission originates in a spiral galaxy 2.0 h_{65}^{-1} megaparsecs from the cluster core. No other significant detections have been made in the cluster, suggesting that the mechanisms that remove neutral gas from cluster galaxies are efficient. We infer that fewer than three gas-rich galaxies were accreted by Abell 2218 over the past 10^9 years. This low accretion rate is qualitatively consistent with low-density cosmological models in which clusters are largely assembled at $z > 1$.

Galaxies in clusters have evolved in the past ~3 × 10^9 years. The number of blue galaxies in clusters was higher in the past (the Butcher-Oemler effect) (*1*, *2*) and spiral galaxies were more prevalent (*3*–*5*). It has been argued that these effects are caused by enhanced accretion of gas-rich star-forming galaxies from the surrounding field (*6*–*8*). Detailed modeling suggests that the neutral gas disks of infalling galaxies can be stripped by the hot x-ray gas that envelopes rich galaxy clusters (*9*–*11*). Because the neutral gas provided the fuel for star formation, the star formation rate drops precipitously after the cold gas has been removed. Hence, galaxies rapidly fade and redden after they have been accreted by a rich cluster. The low neutral atomic hydrogen (HI) content of galaxies in the cores of the nearby Coma (*12*) and Virgo (*13*) clusters is consistent with these models. However, at higher redshift, at which the galaxy accretion rate is predicted to be higher and spiral galaxies are more abundant in the central regions of rich clusters, these models have not been tested by direct observations of the neutral gas reservoir of infalling galaxies. Studies of HI at an emission line of 21 cm wavelength have been limited to the local universe (*12*–*15*), because radio synthesis telescopes were not equipped to operate at frequencies corresponding to the redshifted HI line or lacked the sensitivity to detect the HI line at higher redshifts.

We have initiated a program of deep HI imaging of galaxy clusters Abell 2218 and Abell 1689 at redshift (z) ~ 0.2 to study the content and distribution of HI in cluster galaxies at intermediate redshifts. Here, we report on observations of Abell 2218 at z = 0.176 from the recently upgraded Westerbork Synthesis Radio Telescope (WSRT). The cluster is extremely rich and massive (*16*, *17*), has a luminous and extended x-ray halo (*18*), and has become widely known for the Hubble Space Telescope imaging that revealed a rich structure of strong gravitational arcs (*19*).

Observations were performed with the WSRT during the commissioning of the upgraded system in the period from July to

[1]School of Physics, University of Melbourne, Victoria 3010, Australia. [2]California Institute of Technology, Mail Stop 105-24, Pasadena, CA 91125, USA. [3]Department of Astronomy, University of Wisconsin, 475 North Charter Street, Madison, WI 53706, USA. [4]National Radio Astronomical Observatory, Post Office Box 0, Socorro, NM 87801, USA.

*To whom correspondence should be addressed. E-mail: mzwaan@physics.unimelb.edu.au